Laser and Particle Beams (2000), *18*, 145–150. Printed in the USA.

Experimental study of picosecond laser plasma formation in thin foils

M. GALIMBERTI,[1] L.A. GIZZI,[1] A. BARBINI,[1] P. CHESSA,[2]
A. GIULIETTI,[1] D. GIULIETTI,[3] AND A. ROSSI[1]

[1]Istituto di Fisica Atomica e Molecolare, Area della Ricerca del CNR, Via Alfieri, 1, 56010 Ghezzano, Pisa, Italy
[2]LOA-ENSTA, Ecole polytechnique, 91128 Palaiseau cedex, France
[3]Dipartimento di Fisica, Università di Pisa, and INFM, via Buonarroti, 2, 56100 Pisa, Italy

(RECEIVED 27 January 1999; ACCEPTED 17 February 1999)

Abstract

A high performance, fully controlled picosecond laser system has been designed and built with the aid of a numerical code capable of simulating the temporal behavior of the laser system, including each active and passive component. The laser performance was characterized with an optical streak camera, equivalent plane monitor, and calorimeter measurements. The laser pulse was focused on 150-nm thick foils to investigate plasma formation and the related transmittivity of the laser light. The experimental data are in very good agreement with the predictions of a simple, 2D analytical model that takes into account the actual shot-to-shot features of the laser pulse. The temporal profile of the pulse and the intensity distribution in the focal spot were found to play a key role in determining the transmission properties of the laser-irradiated foil. This work may be relevant to a wide class of laser exploded foil plasma experiments.

1. INTRODUCTION

Plasmas produced by laser explosion of thin foils have been intensively investigated so far, due to the wide range of their potential applications, running from X-ray lasers (Matthews *et al.*, 1985) to ICF related laser interaction tests with performed plasmas (Seka *et al.*, 1992). The technique of thin foil laser irradiation has been applied to a variety of experimental conditions of laser-matter interactions from nanosecond (Giulietti A. *et al.*, 1989; Willi *et al.*, 1990, Gizzi *et al.*, 1994 and references therein) to femtosecond pulses (Gizzi *et al.*, 1996). These experiments have shown a remarkably rich variety of physical phenomena, including the recent observation of the transmission of high intensity fs laser pulses through an overdense plasma (Giulietti *et al.*, 1997; Fuchs *et al.*, 1998). An important effort has been devoted to characterizing the long scalelength plasma produced from thin foils irradiated with ns pulses (Gizzi *et al.*, 1994; Borghesi *et al.*, 1994) for a better comprehension of the laser interaction physics with such a preformed plasma.

A specific problem to be studied is the mechanism of initial plasma formation for a given laser intensity (threshold) which depends on many factors, including pulse length and foil thickness. In particular, the dependence on the pulse length is due to the different processes that can occur at different timescales. This kind of study has a clear relevance for the understanding of fundamental phenomena such as laser field ionization and electron acceleration, avalanche breakdown of materials, surface waves, and so on.

Particular attention must be devoted in these experiments to the laser pulses used which, regardless of their duration (ns, ps, or fs), are usually characterized by longer prepulses, which can produce a premature plasma formation, and consequently change the interaction physics. In the case of fs laser-foil interactions, both ns (due to the amplified spontaneous emission—ASE) and ps pedestals are usually present; then the plasma formation threshold has to be investigated in both the ns and the ps regime.

In this paper we present a study of plasma formation in 150-nm-thick FORMVAR ($C_5H_{11}O_2$) targets. An important feature of our targets is that they do not absorb the Nd:Yag laser at low intensity. In other words, at laser intensities below the plasma formation threshold the incident laser intensity is either transmitted or reflected. This was tested experimentally over a wide range of laser intensities. Particular attention was devoted to the control of the laser system and to as complete as possible a characterization of the laser parameters in the focal region. To this purpose we have designed a high-performance ps laser system with the aid of a numerical code. The pulse length, measured with an optical streak-camera, was found to be typically 40 ps; the pulse

Address correspondence and reprint requests to: M. Galimberti, Istituto di Fisica Atomica e Molecolare, Area della Ricerca del CNR, Via Alfieri, 1, 56010 Ghezzano, Pisa, Italy. E-mail: marco@plasma.ifam.pi.cnr.it

energy was monitored shot-by-shot with a calorimeter; an equivalent plane monitor gave the shot-by-shot laser intensity distribution on target. The focal spot was found to be very close to the one expected for a diffraction-limited beam. The level of transmittivity of the laser light through the foil was measured at different laser intensities for two different angles of incidence. The experimental data are compared with an analytical model and discussed.

2. LASER REQUIREMENTS AND DESIGN

As we were interested in the investigation of the ps regime of plasma formation, we designed a mode-locked laser system, whose oscillator performance was improved by the simultaneous action of a passive dye saturable absorber and an active acousto-optic modulator crystal (AOM). This allowed us to obtain a laser pulse characterized by a smooth temporal profile, free from unknown secondary spikes and a focal spot profile free from hot spots. These aspects play a key role in the investigation of processes whose growth and evolution depend strongly on the local laser's intensity.

The numerical code MOLOC (Galimberti, 1998) was developed to simulate the laser output as a function of parametric changes of each component of the oscillating cavity. The performance of the single components of the oscillator cavity, namely the dye cell and the AOM, were modeled on the basis of published data. The predictions of the code were found to be in good agreement with the actual behavior of the system, and made it possible to identify the role played by the two main mode-locking components. The conclusions are that the AOM acts mainly in synchronizing the system while the dye generates the train of pulses and fixes the pulse duration and energy.

Figure 1 shows the code outputs for a realistic choice of the parameters. The pulse train is shown in (a). Early in the train each pulse barely emerges from a chaotic set of pulses (b); the contrast ratio between each pulse and the background increases as the train evolves (c), and a "clean" pulse appears on the top of the train (d). A log-scale view of the pulse (e) shows the presence of a ns low-power pedestal. The detailed temporal profile of the simulated main pulse is shown in (f). In general, the laser output and the simulations were found in good qualitative agreement, though an absolute comparison would require a detailed knowledge of the characteristics of both AOM and dye. The code however, was very useful in setting and optimizing the system parameters.

3. LASER OUTPUT CHARACTERIZATION

With the laser cavity parameters optimized and single-pulse operation selected, pulse duration measurements were carried out by means of an optical streak camera. Since the camera was equipped with an S11 photo-cathode, the laser pulse was frequency doubled using a doubling crystal. A fraction of the pulse was relayed on the entrance slit of the camera, streaked and detected using a CCD imaging system. From such an image the temporal profile of the second harmonic pulse was obtained after removal of the CCD nonlinearity and background, integration over the spatial axis (perpendicular to the time-axis) and calibration of the time-axis scale. The final profile was then fitted with a Gaussian function. The result is shown in Figure 2. The duration of the original infrared pulse was obtained from the 2ω measurements assuming that in the regime of low 2ω conversion efficiency $I_{2\omega} \propto I_{\omega}^2$, and consequently $\Delta t_{\omega} = \Delta t_{2\omega} \cdot \sqrt{2}$, where Δt is the pulse full width half maximum (FWHM). This condition is satisfied in our case since it was verified experimentally that the 2ω conversion efficiency was $\approx 10^{-3}$. The temporal profile of the pulse was found to be well described by a Gaussian function of maximum intensity I_M superimposed on a background intensity I_B:

$$I(t) = I_B + I_M \cdot \exp\left[-4 \cdot \ln 2 \cdot \left(\frac{t - t_c}{\Delta T}\right)^2\right], \tag{1}$$

where t_c is the temporal position of the maximum of the Gaussian function. Also, the statistical distribution of the pulse duration over a large number of shots was investigated. From the experimental distribution we found a pulse duration $\Delta T = 44.6 \pm 7.1$ ps.

The oscillator output is amplified up to 200 mJ per pulse by a three-stage glass amplifier chain, and then focused on the target by an F/8 optics. The intensity distribution in the focal plane was monitored shot-by-shot by an equivalent plane monitor based on a 300-cm focal length lens which gave a magnified image of the spot on a CCD detector. A typical image of the focal spot as obtained from the equivalent plane monitor is given in Figure 3. It shows a focal spot very close to the diffraction limit, whose radial profile is well fitted by a Gaussian function plus a uniform background:

$$I(x, y) = I_B + I_M \cdot \exp\left\{-2 \cdot \left[\left(\frac{x - x_c}{w_x}\right)^2 + \left(\frac{y - y_c}{w_y}\right)^2\right]\right\}. \tag{2}$$

The fit gives waist parameters $w_x = 6.39 \pm 0.33$ μm and $w_y = 5.21 \pm 0.29$ μm.

4. TRANSMISSION AND SELF-EMISSION MEASUREMENTS

Plasma formation on 150-nm thick plastic (FORMVAR) foils was investigated by measuring the transmittivity of the target as a function of the laser pulse energy. The transmitted laser energy was measured by imaging the back-side of the foil on a CCD camera, along the beam axis, with the same solid angle of the laser focusing lens. At the same time, the intensity of optical self-emission from the interaction region was measured at an angle of 50° with respect to the laser beam axis

https://doi.org/10.1017/S0263034600181170 Published online by Cambridge University Press

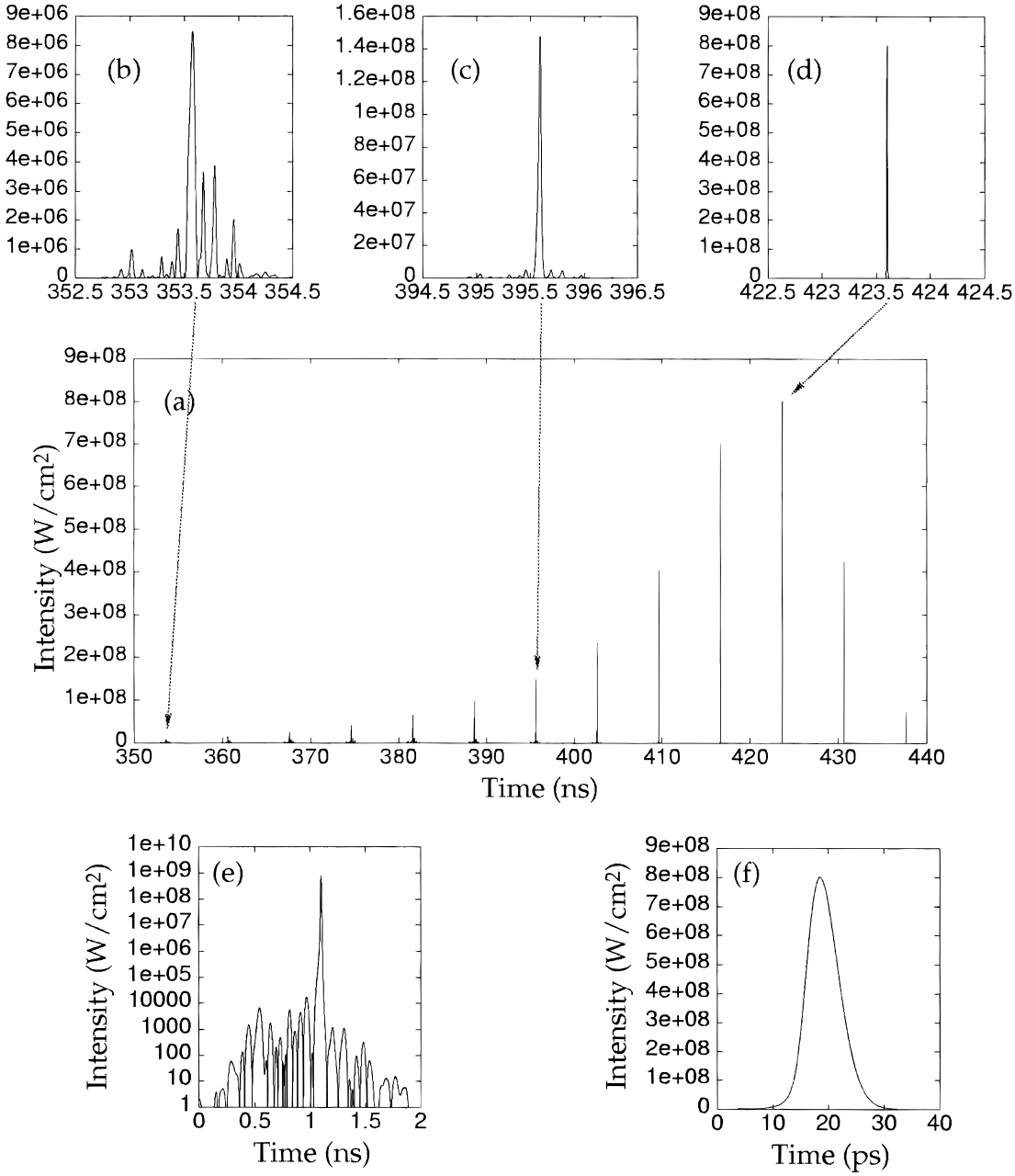

Fig. 1. Output of the simulation code MOLOC showing the behavior of the laser pulse generated by the passive-active mode-locked laser cavity. The pulse train is shown in (a). Early in the train each pulse barely emerges from a chaotic set of pulses (b); the contrast ratio between each pulse and the background increases as the train evolves (c), and a "clean" pulse appears on the top of the train (d). A log-scale view of the pulse (e) shows the presence of a ns low-power pedestal. The detailed temporal profile of the simulated main pulse is shown in (f).

and integrated over the entire spectral region of sensitivity of the CCD detector (400–800 nm). Measurements were performed at two angles of incidence of the laser on the foil, namely at 0.9° and 14.4°, with the laser light linearly *p* polarized. The plots of the transmitted energy versus the incident laser pulse energy for the case of 0.9° and 14.4° angles of incidence are shown in Figure 4 and Figure 5 respectively.

According to these plots, as the incident laser energy increases, the transmitted energy increases linearly up to a certain value the behavior changes dramatically, showing a constant transmittivity as expected in the case of optical (cold target) transmission. Above this value the behavior changes dramatically, the transmitted laser energy tends to saturate indicating a change of the transmission properties of the target. The plot of the self-emission intensity as a function of

https://doi.org/10.1017/S0263034600181170 Published online by Cambridge University Press

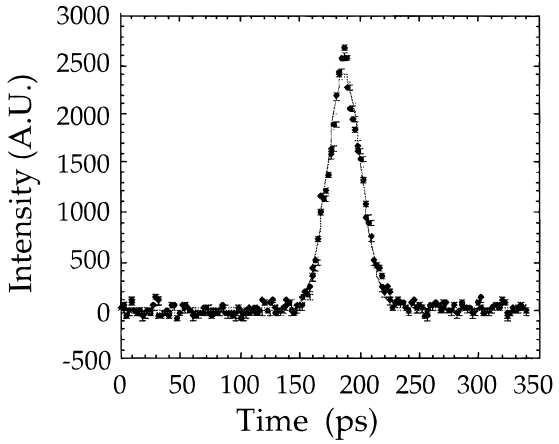

Fig. 2. Reconstructed temporal profile of the laser pulse obtained from streak-camera measurements. The pulse frequency was doubled and measured with an optical streak-camera. The duration of the infrared pulse was obtained from the 2ω measurements assuming that in the regime of low 2ω conversion efficiency $I_{2\omega} \propto I_{\omega}^2$, and consequently $\Delta T_{\omega} = \Delta T_{2\omega} \cdot \sqrt{2}$, where ΔT is the pulse FWHM.

the incident laser pulse energy is shown in Figure 6. The emission from the interaction region, in the case of a 0.9° angle of incidence, does not emerge appreciably from the background level for the entire incident energy range. In contrast, in the case of a 14.4° angle of incidence, a rapid growth of the self-emission intensity is observed at a well-defined value of the incident energy.

5. ANALYTICAL MODEL AND DISCUSSION

A simple model of laser induced plasma formation has been considered in order to explain our experimental data on foil

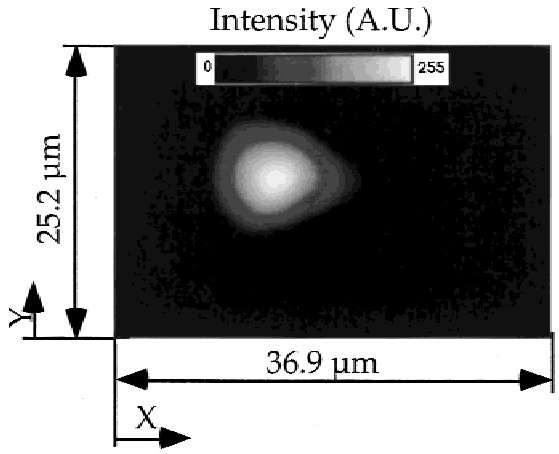

Fig. 3. A typical image of the focal spot as obtained from the equivalent plane monitor based on a 300-cm focal length lens which gave a magnified image of the spot on a CCD detector.

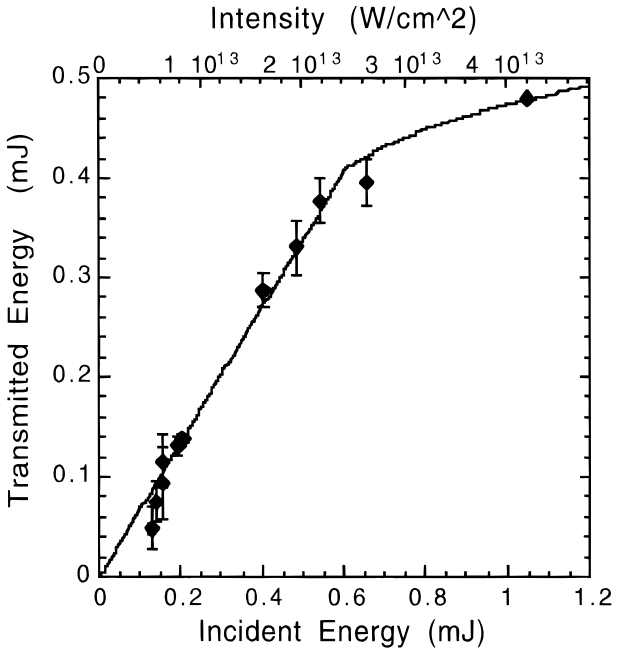

Fig. 4. Energy transmitted through 150-nm-thick plastic foils as a function of the incident laser energy. The 40 ps laser pulse was focused on target in a 6-μm FWHM focal at an angle of incidence of 0.9 degrees. The solid curve shows the calculated transmittivity as obtained from a simple analytical 2D model (see text).

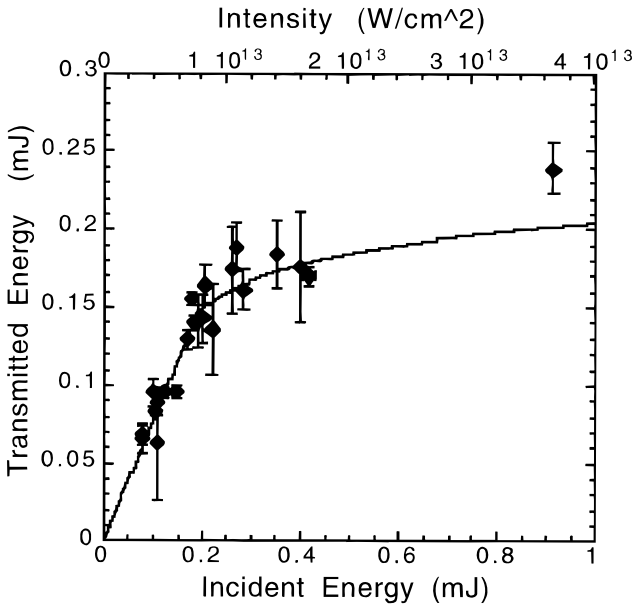

Fig. 5. Energy transmitted through 150-nm-thick plastic foils as a function of the incident laser energy. The 40 ps laser pulse was focused on target in a 6-μm FWHM focal at an angle of incidence of 14 degrees. The solid curve shows the calculated transmittivity as obtained from a simple analytical 2D model (see text).

https://doi.org/10.1017/S0263034600181170 Published online by Cambridge University Press

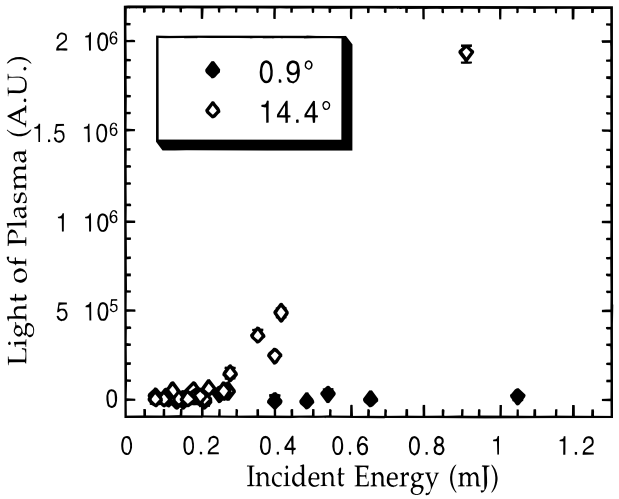

Fig. 6. Level of self-emission from the region of interaction of a 40 ps laser pulse with 150-nm thick plastic foil. The laser pulse was focused in a 6-μm FWHM focal spot at two different angles of incidence, namely 0.9 degrees and 14 degrees.

transmittivity. The region of the laser interaction with the foil has been assumed to have a circular symmetry around the laser beam axis (maximum intensity) with a radial coordinate r. Since the target does not absorb laser energy at low intensity, we can assume that for laser intensities below a threshold intensity I_{th} the local transmittivity is given by the dielectric transmittivity of the foil. Above this value the foil is ionized instantaneously (i.e., in a time much shorter than the laser pulse duration) to a density of free electrons higher than the critical density. After ionization, the incident laser light is totally reflected and/or absorbed by the plasma.

In the simplest case of a spatially uniform spot and a Gaussian temporal profile $I(t) = I_M \cdot \exp(t/\tau)^2$, the transmitted energy is given by

$$E_T = \begin{cases} \frac{1}{2} \cdot \delta \cdot E_I \cdot \text{erfc}\left(\sqrt{\ln\left(\frac{\delta \cdot E_I}{E_{\text{th}}} \right)} \right) & \delta \cdot E_I \geq E_{\text{th}} \\ \delta \cdot E_I & \delta \cdot E_I < E_{\text{th}} \end{cases}, \quad (3)$$

where E_T is the transmitted energy, δ is the optical transmittivity of the target, E_I is the incident energy and $E_{\text{th}} = \sqrt{\pi} \cdot I_{\text{th}} \cdot s \cdot \tau$, s being the area of the focal spot. However, since in our case the detailed laser intensity distribution in the focal plane is well known, we can include it in our model. From the characterization of the laser output in section 3, we know that the intensity in our focal spot has a nearly Gaussian radial profile $I(r,t) = I_M \cdot \exp(t/\tau)^2 \cdot \exp[-2 \cdot (r/w)^2]$. Consequently, the transmitted energy in our case can be written as:

$$E_T = \begin{cases} \frac{1}{2} \cdot E_{\text{th}} \cdot \left[1 + \frac{2}{\sqrt{\pi}} \cdot \sqrt{\ln\left(\frac{\delta \cdot E_I}{E_{\text{th}}} \right)} \right. \\ \qquad \left. + \frac{\delta \cdot E_I}{E_{\text{th}}} \cdot \text{erfc}\left(\sqrt{\ln\left(\frac{\delta \cdot E_I}{E_{\text{th}}} \right)} \right) \right] & \delta \cdot E_I \geq E_{\text{th}} \\ \delta \cdot E_I & \delta \cdot E_I < E_{\text{th}} \end{cases} \quad (4)$$

where $E_{\text{th}} = (\sqrt{\pi^3}/2) \cdot w^2 \cdot \tau \cdot I_{\text{th}}$.

The calculated behavior of the transmitted energy as a function of the incident laser energy as given by the two models 3 and 4, is shown in Figure 7. Clearly, the case of uniform intensity gives a rather unrealistic result, with a discontinuity in the transmitted energy at $I = I_{\text{th}}$. On the contrary, in the case of the Gaussian profile, the general behavior agrees well with the trend of our experimental data, showing a linear dependence for values below I_{th} and saturation above I_{th}. A quantitative comparison between the model and our data has been carried out also taking into account the angle of incidence (and the resulting elliptical spot). The intensity distribution on target in this case is given by

$$E_{\text{th}} = \frac{\sqrt{\pi^3}}{2} \cdot \frac{w_x}{\cos(\alpha_{\text{Inc}})} \cdot w_y \cdot \tau \cdot I_{\text{th}}, \quad (5)$$

where

$$\tau = \frac{\Delta T}{2 \cdot \sqrt{\ln 2}} = 26.8 \pm 7.3 \text{ ps},$$

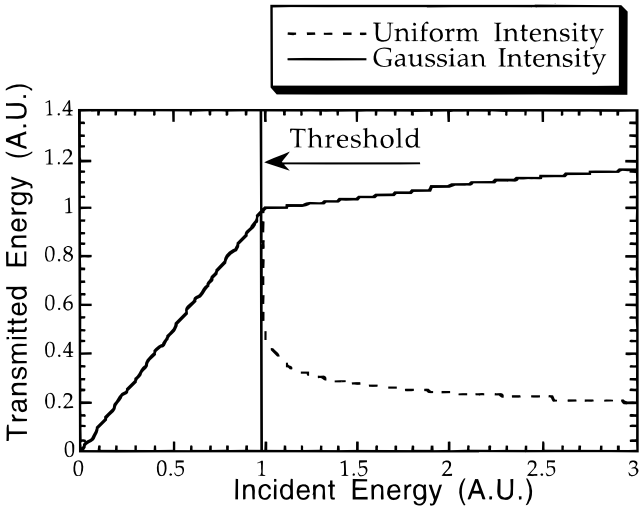

Fig. 7. Transmitted energy *versus* incident laser energy as predicted by a simple 2D analytical model of transmittivity (see text). The dashed line corresponds to the case of uniform laser intensity in the focal spot while the solid line corresponds to a more realistic situation of Gaussian intensity distribution in the focal spot.

https://doi.org/10.1017/S0263034600181170 Published online by Cambridge University Press

Table 1. *Experimental values of the parameters included in the model of Eq. 4 as resulting from the best fit of the data in Figures 4 and 5.*

	0.9°	14°
δ	0.676 ± 0.031	0.770 ± 0.030
E_{th}	0.410 ± 0.036 mJ	0.146 ± 0.014 mJ
I_{th}	16.5 ± 3.3 TW/cm^2	5.9 ± 1.2 TW/cm^2
χ^2	5.9	51.1
N_{df}	9	20

and α_{Inc} is the angle of incidence. The "cold target" (optical) transmittance δ and the plasma formation energy E_{th} were left as free parameters and were obtained by the best fit of this curve to our data. The calculated transmittances obtained from this model in the case of Gaussian profile, at 0.9° and 14.4° angles of incidence are shown by the solid curves of Figures 4 and 5 respectively, while the corresponding values of the optical transmittivity and the plasma formation laser intensity (and energy per pulse) are given in Table 1.

The values of "cold target" transmittivity correspond to the values found from separate optical measurements performed at very low laser intensity in which no absorption within the sample was observed. An additional feature of these results is that the value of the plasma formation threshold, I_{th} at normal incidence is found to be considerably higher than in the case of 14° angle of incidence. This interesting behavior is now under investigation. Another important point concerns the behavior of self-emission from the interaction region which is often used as a marker of plasma formation. Our measurements indicate that self-emission becomes appreciable only at laser energies substantially higher than E_{th}. These circumstances could lead to an overestimation of the plasma formation threshold.

6. CONCLUSION

A fully controlled mode-locked ps laser oscillator cavity was built with the aid of a specifically designed numerical code. The pulse was amplified to the multi-GW level by a three-stage glass amplifier chain. Both the temporal profile and the far field intensity distribution of the laser pulse were monitored and were found to be well described by Gaussian functions. Measurements of the transmittivity of a thin plastic foil to ps laser pulses provide evidence of a well-defined intensity threshold for dense plasma formation which strongly depends on the angle of incidence. This threshold is lower than what can be inferred from the simple observation of self-emission from plasma formation. A simple analytical model has been proposed whose predictions are in good agreement with the observed behavior and allows the threshold intensity to be measured accurately.

REFERENCES

Borghesi, M. *et al.* 1994, *Phys. Rev. E* **49**, 5628.
Fuchs, J. *et al.* 1998, *Phys. Rev. Lett.* **80**, 2326.
Galimberti, M. 1998, IFAM Report **5/98**.
Giulietti, A. *et al.* 1989, *Phys. Rev. Lett.* **63**, 524.
Giulietti, D. *et al.* 1997, *Phys. Rev. Lett.* **79**, 3194.
Gizzi, L.A. *et al.* 1994, *Phys. Rev. E* **49**, 5628 and references therein.
Gizzi, L.A. *et al.* 1996, *Phys. Rev. Lett.* **76**, 2278.
Matthews, D.L. *et al.* 1985, *Phys. Rev. Lett.* **54**, 110.
Seka, W. *et al.* 1992, *Phys. Fluids. B* **4**, 432.
Willi, O. *et al.* 1990, *Phys. Fluids B* **2**, 1318.

https://doi.org/10.1017/S0263034600181170 Published online by Cambridge University Press